Spatially Resolved Proteomics Reveals Lens Suture-Related Cell–Cell Junctional Protein Distributions

Zhen Wang, Romell B. Gletten, and Kevin L. Schey

Department of Biochemistry and Mass Spectrometry Research Center, Vanderbilt University School of Medicine, Nashville, Tennessee, United States

Correspondence: Kevin L. Schey, Department of Biochemistry, Mass Spectrometry Research Center, 465 21st Ave So., Suite 9160 MRB III, Nashville, TN 37232, USA; kevin.schey@vanderbilt.edu.

Received: May 17, 2023
Accepted: July 31, 2023
Published: August 21, 2023

Citation: Wang Z, Gletten RB, Schey KL. Spatially resolved proteomics reveals lens suture-related cell–cell junctional protein distributions. *Invest Ophthalmol Vis Sci.* 2023;64(11):28. https://doi.org/10.1167/iovs.64.11.28

Purpose. Lens transparency relies on the precise organization of lens fiber cells. The formation of the highly ordered lens architecture results from not only cell–cell adhesion along the lateral interfaces, but also from proper organization of fiber cells tips at lens sutures. Little is known about the cell adhesion between fiber tips at the sutures. The purpose of this study is to map suture-specific protein distributions.

Methods. Tissue sections were obtained from fresh frozen bovine lenses and washes were performed to remove soluble proteins and to retain membrane and membrane associated proteins. Imaging mass spectrometry (IMS) combined with on-tissue trypsin digestion was used to visualize protein spatial distributions. Sutures and adjacent regions were captured by laser capture microdissection and samples were digested by trypsin. Proteins were analyzed by liquid chromatography tandem MS and quantified by label-free quantification. Protein spatial distributions were confirmed by immunofluorescence.

Results. IMS results showed enrichment of adherens junction proteins cadherin-2 and armadillo repeat gene deleted in velo–cardio–facial syndrome (ARVCF) in both anterior and posterior sutures of bovine lenses. Liquid chromatography tandem MS confirmed higher expression of cadherin-2 and ARVCF and other adherens junction proteins including catenin $\alpha 2$ (CTNNA2) and catenin $\beta 1$ (CTNNB1) in sutures. In contrast, IMS indicated low expression of gap junction protein connexin 50 and connexin 46 in the suture regions. The localization of cadherin-2 and connexin 50 was confirmed by immunofluorescence.

Conclusions. The complementary expression of adherens junction proteins and gap junction proteins in lens suture regions implicates adherens junctions in fiber cell tip adhesion and in maintaining the integrity of the lens.

Keywords: suture, MALDI imaging, adherens junction, gap junction

The ocular lens has a relatively simple cellular composition with a monolayer of epithelial cells underlying the anterior portion of the lens capsule and the lens fiber cells forming the bulk of the lens. Although cellularly simplistic, lens fiber cells are precisely organized, resulting in a highly ordered lens architecture that is important for maintaining lens transparency. Throughout life, epithelial cells differentiate continuously into fiber cells in the equatorial region of the lens. Fiber cell differentiation is characterized by precise migration and extensive elongation.[1,2] During elongation, the apical fiber tips extend beneath the epithelium monolayer and the basal tips migrate beneath the posterior lens capsule until their tips touch the fiber cell tips from the opposite hemisphere of the lens to form anterior and posterior sutures.[3–6] When the anterior and posterior ends of a group of same aged fiber cells all reach the suture lines, a growth shell is formed.[4,5] Fiber cells in different growth shells are in different stages of differentiation and are of a different age. Within a growth shell, fiber cells have diverse migration paths, resulting in fiber cells with different curvatures and variable lengths.[4] The programmed end-to-end arrangement of fiber cells within and between concentric growth shells forms specifically shaped sutures.[4] Different suture patterns across species contribute to the different optical qualities of the lens[7] and may affect the range of accommodation.[4]

Accompanying the high order of fiber cell organization, different cellular morphology and characteristic membrane architecture occur in different lens regions.[8,9] During differentiation, fiber cells undergo dramatic changes, including the loss of cellular organelles and increased synthesis of lens specific proteins.[1] Using laser capture microdissection (LCM) and quantitative mass spectrometry (MS), lens fiber cells were found to undergo remarkable proteome changes, including membrane and cytoskeletal remodeling in a narrow region of the lens cortex.[9,10] Gene expression in single fiber cells collected from different regions of the lens was also studied and heterogeneity of gene expression in cortical fiber cells was reported.[11] In addition, significant progress has been made in identifying and characterizing the variation of posttranslational modifications in the different regions of the lens.[12–20] Based on these data and other spatially resolved analyses of lens proteins, a highly spatially regulated protein distribution is expected to be present in

the lens. Previous studies of differential lens protein expression focused on proteome changes in the different lens regions corresponding with age-related concentric growth shells; typically, only the equatorial region of the lens was studied.[15–20] Lens suture formation is an important part of highly ordered lens architecture, and the abnormal development of sutures has been shown to be associated with specific types of cataract.[4] Sutures also play important roles in the lens microcirculation system.[21–23] However, other than a few proteins such as AQP0[24] and lactase-like protein (LCTL, KLPH)[25] that were reported to be involved in suture development, to the best of our knowledge, very few studies have examined protein distributions in lens sutures.[3,26] Previously, a cytoskeletal assembly that is structurally and compositionally analogous to classical terminal webs that abut at sutures was described, but the cell adhesion properties between fiber tips at sutures remain unknown.[2,26] It is expected that fiber cells may develop differential protein distributions with suture-specific patterns, especially for proteins involved in cell adhesion and cell–cell junctions.

Imaging MS (IMS) is a rapidly developing technology that enables the untargeted investigation of the spatial distribution of biological molecules.[27] With IMS, mass spectra that contain hundreds or thousands of signals are collected at discrete spatial points and the results can simultaneously provide the spatial distributions of thousands of molecules. The sensitivity of IMS for intact proteins is generally low and intact protein imaging is limited to abundant proteins and small proteins with a molecular weight less than approximately 30 kDa.[28] Therefore, an on-tissue digestion method was developed to convert large proteins to easily detectable peptides without changing their spatial distribution.[29] In this article, we applied IMS combined with on-tissue digestion to study the differential membrane protein distribution in anterior and posterior equatorial bovine lens sections. Our results showed complementary patterns of adherens junction proteins (N-cadherin and armadillo repeat gene deleted in velo–cardio–facial syndrome [ARVCF]) and gap junction proteins (connexin 50 and connexin 46) in suture regions. To confirm the IMS data, LCM was used to capture suture regions and regions adjacent to the sutures, and quantitative liquid chromatography tandem MS (LC-MS/MS) analysis was performed. In addition, immunofluorescence was also performed to further verify the results.

Materials and Methods

Tissue Preparation for IMS

Bovine lenses were extracted from fresh cow eyes (Light Hill Meats, Lynnville, TN, USA) and frozen at –80°C. Each lens was sectioned equatorially to 12 µm thickness using a CM 3050 Cryostat (LEICA CM 3050S, Leica Microsystems Inc., Bannockburn, IL, USA). Equatorial sections were collected from both anterior and posterior regions. All sections were collected at a distance of 700 to 1000 µm from the anterior or posterior pole. A diagram that shows the regions where sections were collected and the dimensions of a bovine lens is included in Supplementary Figure S1. Note that all sections were collected from the regions close to the anterior or posterior pole; therefore, the fiber cells even in the center of the sections are still young fiber cells. Sections were thaw-mounted on indium–tin–oxide (ITO)–coated slides (Delta Technologies, Loveland, CO, USA). All ITO slides were treated with sodium carbonate solution as described previously.[30] After sections on ITO slides were dry, the sections were washed sequentially as follows: 50 mM ammonium formate wash for 2 minutes, followed by drying in a vacuum desiccator and repeated once, water wash for 1 minute and dried, 4 M urea wash for 1 minute followed by three water washes for 1 minute and dried, 8 M urea wash for 1 minute followed by three water washes for 1 minute and dried, 10 mM NaOH wash for 1 minute followed by three water washes and dried, and 95% ethanol wash for 2 minutes twice and dried. On-tissue digestion was performed as described previously.[30] Briefly, the sections were sprayed with trypsin (15 ng/µL in 10% ACN in 100 mM ammonium bicarbonate, pH 8) using a TM Sprayer (HTX Technologies, Carrboro, NC, USA) modified with a syringe pump at 8 µL/min (Harvard Apparatus, Holliston, MA, USA). Trypsin was applied in eight passes with nozzle velocity of 750 mm/min at 30°C. The final trypsin concentration on tissue was 0.64 ng/mm^2. Digestion was done in a sealed humidified petri dish at 37°C with 0.1 mL 100 mM ammonium bicarbonate for 4 hours. After digestion, the sections were sprayed with 2,5-dihydroxybenzoic acid (10 mg/mL, 90% ACN, 0.1% TFA) in eight passes using the TM sprayer (85°C, 0.1 mL/min flow rate, 700 mm/min velocity, 2-mm track spacing, nitrogen carrier gas 9.5 psi).

IMS Data Acquisition

Imaging experiments were performed using a Bruker SolariX 15T FT-ICR mass spectrometer (Bruker Daltonics, Billerica, MA, USA) in positive ion mode. Images were acquired using a Smartbeam II 2 kHz Nd:YAG (355 nm) laser using a small laser setting (estimated spot size of approximately 50 µm) with 500 laser shots per pixel with a raster step size of 75 µm. The mass spectrometer was externally calibrated before analysis using a peptide mixture (Leu-enkephalin, Angiotensin II, Fibrinopeptide B, ACTH fragment [1–24], and insulin chain B). The mass spectrometer was operated in positive ion mode and data were collected from m/z 500 to 4000 at a mass resolution of approximately 125,000 at m/z = 1046.542.

Immunofluorescence

For immunofluorescence, bovine lenses were fixed and cryoprotected as described previously.[31] We collected 20-µm sections on regular glass slides in PBS. The sections were washed with PBS and incubated with blocking solution containing 6% BSA and 6% normal goat serum in PBS for 1.5 hours. The sections were then incubated with rabbit anti-cadherin 2 (CDH2) (1:200) (Thermo Fisher Scientific, Waltham, MA, USA; PA5-19486) or mouse anti-connexin 50 (1:100) (Thermo Fisher Scientific, #33-4300) for 16 hours at 4°C. The sections were washed with PBS to remove unbound primary antibodies and further incubated with Alexa488-conjugated goat anti-rabbit (1:400) for cadherin and Alexa647-conjugated goat anti-mouse (1:200) for connexin 50 for 2 hours. The sections were washed with PBS to remove excess secondary antibodies, followed by incubation with Alexa488- or Alexa647-conjugated wheat germ agglutinin (1:100) for 1 hour to label fiber cell plasma membranes. The sections from fixed lenses were washed with PBS and coverslipped in ProLong Gold Antifade Mountant and imaged using a Zeiss LSM 880 confocal laser scanning

Investigative Ophthalmology & Visual Science

microscope (Carl Zeiss Inc; White Plains, NY, USA) or a ZEISS Axio Scan.Z1 (Carl Zeiss Inc; White Plains, NY, USA) high-resolution fluorescence scanner.

LCM and LC-MS/MS Analysis

To identify peptide signals in IMS experiments, 12-µm-thick bovine lens equatorial sections were collected from both anterior and posterior regions. The sections were collected on PEN membrane slides (Carl Zeiss, Munich, Germany) and air dried. The LCM procedure was conducted using a PALM UV Laser MicroBeam LCM system (Carl-Zeiss, Oberkochen, Germany) as described previously.[10] A 200-µm-wide tissue across the anterior or posterior suture regions was captured to generate anterior suture sample A1 as shown in Supplementary Figure S2. A nonsuture region 150 µm wide was captured 200 µm distant from the center of the suture on either side and parallel to the suture line. The samples on either side of the suture were pooled to generate anterior nonsuture sample A2. Similar regions were also captured from posterior regions to generate posterior suture sample P1 and nonsuture sample P2. Approximately 15 mm^2 tissue was collected from each region in total and the samples were dried in a speedvac.

Twenty microliters of 50 mM Tris, 4 M urea, and 10 mM TCEP (pH 8.0) were added to each sample and the samples were incubated at 25°C for 45 minutes. Two microliters of 500 mM iodoacetamide were added to each sample to alkylate free cysteines. The samples were incubated at 25°C for 45 minutes. The samples were then centrifuged at 20,000×*g* for 5 minutes and the supernatant was collected as the soluble fraction. The remaining pellets were washed with 10 µL of 50 mM Tris, 4 M urea (pH 8.0) twice and the supernatant was pooled as 4 M urea-soluble fraction and an aliquot of the soluble fraction was used for Bradford protein assay (Thermo Fisher Scientific, Rockford, IL, USA). The remaining pellets were digested by endoproteinase Lys-C at 37°C in 50 mM Tris buffer (pH 8.0) for 4 hours followed by trypsin digestion overnight as described previously.[10] The samples were dried in a speedvac after digestion and reconstituted in 0.1% formic acid for StageTip cleaning as described previously.[10] After StageTip cleaning, the samples were dried in a speedvac and reconstituted in 0.1% formic acid for LC-MS/MS analysis.

For LC-MS/MS analysis, samples were separated on a one-dimensional fused silica capillary column (250 mm × 100 µm) packed with Phenomenex Jupiter resin (3 µm mean particle size, 300 Å pore size) coupled with an UltiMate 3000 RSLCnano system (Thermo Scientific, San Jose, CA, USA). A 78-minute gradient elution was performed, consisting of the following: 2 to 72 minutes, 2% to 40% ACN (0.1% formic acid); 75 to 78 minutes, 45% to 90% ACN (0.1% formic acid) balanced with 0.1% formic acid. The flow rate was 350 nL/min. The eluate was directly infused into a Q Exactive Plus instrument (Thermo Scientific, San Jose, CA, USA) equipped with a nanoelectrospray ionization source. The data-dependent instrument method consisted of MS1 acquisition (R = 70,000) from m/z 350 to 1600, using an MS AGC target value of 3E6, maximum ion time of 60 ms followed by up to 20 MS/MS scans (R = 17,500) of the most abundant ions detected in the preceding MS scan. The MS2 AGC target value was set to 5E4 with a maximum ion time of 100 ms, HCD collision energy was set to 27, and dynamic exclusion was set to 10 seconds.

Data Analysis

For protein identification, the raw data from LC-MS/MS were loaded in MaxQuant software (http://maxquant.org/, version 1.6.6.0)[32] and searched against a custom bovine database with 20,105 sequences (bovine database downloaded on March 3, 2022) representing one gene per sequence. Contaminant proteins were included using the Andromeda search algorithm within MaxQuant. The following search parameters were used: enzyme, trypsin; maximum missed cleavage, 2; precursor mass tolerance, 5 ppm; and variable modifications, protein N-terminal acetylation and methionine oxidation. The maximum modification on a peptide was 2. A false discovery rate of 1% was applied for both peptide and protein filtering. The label-free quantification (LFQ) algorithm in MaxQuant was used for protein quantitation with match between runs within a 0.7-minute retention time window. Only razor and unique peptides were used for protein-level quantitation. The LFQ intensities of the identified proteins from the MaxQuant searches were imported into Perseus (V1.6.15.0; The Max Planck Institute of Biochemistry, Munich, Germany).[33] Contamination and reverse sequence identifications were filtered, and the remaining protein LFQ intensities were log2 transformed. For quantification, only proteins that were present in 100% of replicates in at least one region were used, and missing values were imputed with random numbers from a normal distribution (width of 0.3 and down shift of 1.8). The Student *t*-test in Perseus was used for identification of significantly changed proteins between regions ($P < 0.05$). A Fisher exact test with a Benjamini–Hochberg corrected false discovery rate of 0.05 was used for identifying enriched Gene Ontology (GO) terms using the total quantified proteins as a background.

For IMS, ion images were generated using FlexImaging software (Version 4.1, Bruker Daltonics, Billerica, MA, USA). Each m/z signal was plotted ±10 ppm and images were displayed using root-mean-square normalization. Data were processed by FTMS processing 2.2.0 (Bruker Daltonics, Billerica, MA, USA) and were imported into SCiLS lab software (version 2017b, SCiLS, Breman, Germany). The imzML file was exported from SCiLS lab and used for protein identification using the HIT-MAP program[34] against a custom bovine lens database that only includes proteins identified from different regions of bovine lenses reported previously[30] and proteins identified in suture and suture surrounding regions in this report. HIT-MAP settings include specific trypsin digestion without missed cleavages, at least two unique peptides for protein identification and 5 ppm mass tolerance.

Results

Sample Preparation and IMS Analysis

As mentioned elsewhere in this article, IMS is a powerful technique to determine the spatial distribution of hundreds to thousands of biomolecules in tissue sections in an untargeted manner. A majority of IMS studies use matrix-assisted laser desorption ionization (MALDI) to ionize molecules present in tissues. However, it is challenging to detect high-molecular-weight, low-abundance proteins as well as membrane proteins by MALDI IMS; therefore, we applied a method of on-tissue digestion to detect tryptic peptides, which are more easily detected than intact proteins.[29] In

Investigative Ophthalmology & Visual Science

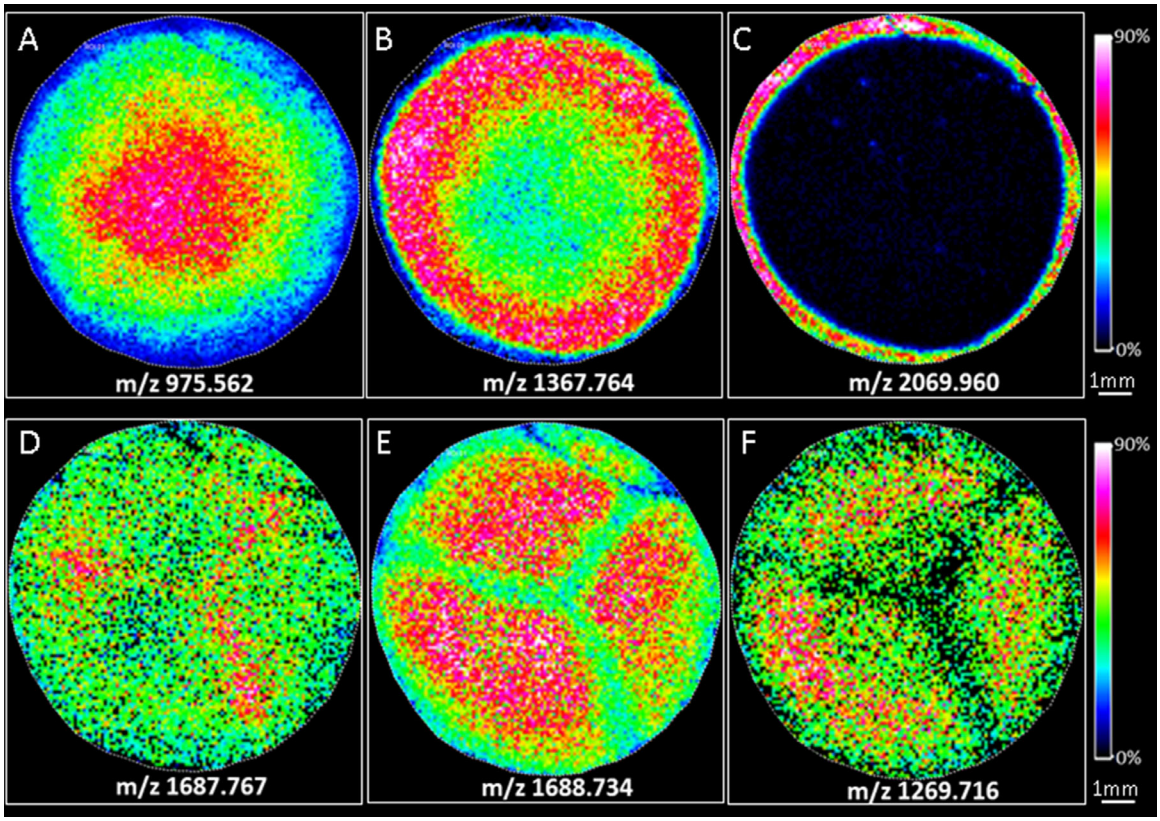

Figure 1. Detected patterns of peptide distributions from IMS data. Six different peptide MALDI images are shown from an anterior section (scale bar, 1 mm). (**A**) AQP0 188–196. (**B**) Spectrin beta 2177–2190. (**C**) AQP0 239–258 with deamidation on Asn246, a truncated form of AQP0. (**D**) ARVCF 587–603. (**E**) connexin 50 110–125 with deamidation on Asn121. (**F**) connexin 50 258–269. The ARVCF sequence used was from the Uniprot database (accession number A0A3Q1LH28).

addition, we captured suture and nonsuture regions by LCM followed by quantitative LC-MS/MS analysis to quantify peptides in these regions and to confirm the IMS results. Last, our focus is on membrane protein localization in the suture regions; therefore, a washing protocol was used to remove highly abundant soluble lens proteins before IMS or LC-MS/MS analysis.

Previously, a method was developed for imaging AQP0, the major membrane protein[17,35]; however, owing to ion suppression from high-intensity AQP0 signals and signals from strongly bound, membrane-associated crystallins, imaging lower abundance membrane proteins in lens tissue is difficult.[17,35] In this study, a more stringent washing protocol was developed, consisting of a combination of urea and a low concentration of sodium hydroxide. The effect of washing can be clearly seen from the mass spectra shown in Supplementary Figure S3. Without washing, only peptides from crystallins were detected. Sections that were washed with a previously reported washing protocol for cytoskeletal proteins[30] showed strong signals from lens beaded filament proteins. After washing with the new membrane washing protocol, mass spectra were dominated by peptide signals from transmembrane proteins AQP0 and connexins (Supplementary Fig. S3). However, the stringent washing poses a challenge for maintaining tissue integrity during washing. Therefore, the protocol also includes optimization of time and sequence of washing. Multiple steps of washing, drying, and gently handling of the sections were found to be essential to maintaining tissue integrity. The goal was to remove crystallins and cytoskeletal proteins in a stepwise manner without decreasing tissue integrity. All washes were performed by gently submerging the slides in a washing buffer with sections lying flat in the solution. Drying the sections after each washing step was found to be very helpful.

After optimization of washing conditions and on-tissue trypsin digestion, peptides were imaged using a high-resolution FT-ICR mass spectrometer. A variety of signal localization patterns were detected, and six of them are shown in Figure 1. The detected patterns indicate that some proteins could be enriched or attenuated in the suture regions, whereas others are not affected by suture structures. For example, signals of AQP0 peptide 188-196 and spectrin beta 2177-2190 showed a concentric distribution corresponding to the age of the fiber cells (Figs. 1A, 1B); however, signals from ARVCF 587-603 and connexin 50 110-125 showed increased and decreased at suture branches, respectively (Figs. 1D, 1E). The spatial distribution of some posttranslational modifications can also be mapped. Nontryptic peptide AQP0 239-258 was detected in only the surface fiber cells (Fig. 1C). The presence of this peptide suggested a cleavage at Leu258. In contrast, the signal of connexin 50 258-269 decreased in the center of the sections, which was due to significantly increased phosphorylation of this peptide (Fig. 1F). The data were analyzed using the HIT-MAP program[34] to identify peptides corresponding to the signals in MALDI imaging data. The results suggested that, other than abundant membrane protein AQP0 and connexins, additional low-abundance transmembrane proteins and peripheral membrane proteins can be detected.

HIT-MAP results revealed 279 unique peptides belonging to 51 proteins detected in posterior region datasets and 221 peptides belonging to 49 proteins were detected in the anterior region datasets. A list of identified proteins can be found in the Supplementary Table S1. Combining both anterior and posterior datasets, 77 proteins were detected, including 39 cytoskeletal and peripheral membrane proteins and 9 transmembrane proteins (Supplementary Table S1). To confirm the identifications, peptides identified by HIT-MAP program were compared with peptides identified by LC-MS/MS and 80% of HIT-MAP identified peptides were detected by LC-MS/MS analysis (Supplementary Table S1).

IMS Analysis Shows Suture-Related Protein Expression Regulation

As shown in Figure 1, IMS analysis detected suture-related protein abundance changes. Multiple signals were detected that were more abundant in the Y-shaped sutures. Signal identification by HIT-MAP revealed many of these suture-enriched signals belong to peptides from CDH2 and ARVCF. The identification of these peptides was further confirmed by their tandem mass spectra from LC-MS/MS analysis. More intense signals from CDH2 and ARVCF peptides were detected in the sutures of both anterior and posterior sections compared with adjacent, nonsuture regions. These results have been confirmed using three different bovine lenses. Representative MALDI images of three distinct peptides from CDH2 and ARVCF are shown in Figure 2. In addition to CDH2 and ARVCF, suture-enriched signals were also identified as peptides from flotillin1, flotillin 2, and neuronal cell adhesion molecule. Images of peptides from these proteins in the posterior section can be found in the Supplementary Figure S4. However, owing to low abundance, peptide signals from these proteins were weak and these signals have not been detected in the anterior sections by IMS.

In contrast with CDH2 and ARVCF, IMS showed decreased signals in the suture regions. Most of these signals were identified as peptides from either connexin 50 or connexin 46. Images of some representative connexin peptides are shown in Figure 3. Decreased connexin abundance in the sutures was consistently detected in both anterior and posterior sections. To show the reciprocal images of CDH2, ARVCF, and Cx50 peptides, overlaid signals of CDH, ARVCF, and Cx50 peptides are shown in Figure 4.

LCM-LC-MS/MS Analysis

To verify the suture-related protein abundance changes indicated by IMS results, we used LCM to capture lens tissue from suture regions and adjacent nonsuture regions. Because membrane and membrane-associated proteins are the focus of this study, the samples captured by LCM were washed with Tris buffer containing 4 M urea to partially remove highly abundant crystallins. After trypsin digestion of the insoluble fraction and LC-MS/MS analysis, protein abundance was quantified by a label-free quantification (LFQ) technique,[32] which is a MS-based relative global protein quantification method based on peak intensities of proteolytic peptides. Consistent with IMS data, the abundance of ARVCF and CDH2 was significantly increased in the suture region compared with adjacent nonsuture region in both anterior and posterior regions (Figs. 5A, 5B). Results from LC-MS/MS analysis of gap junction proteins connexin 50 and connexin 46 were not completely consistent with MALDI imaging data. For the anterior sections, connexin 50 was found to be decreased in the suture region and this difference was statistically significant (Fig. 5C). Even though the difference of Cx46 in the suture and nonsuture region did not reach statistical significance, LC-MS/MS analysis also showed a trend consistent with IMS data. Neither Cx46 nor Cx50 showed a significant difference when comparing suture and nonsuture regions in the posterior samples (Fig. 5D), perhaps owing to capture of both suture and nonsuture regions by LCM.

Together with enriched CDH2 and ARVCF, LC-MS/MS analysis also identified an additional 23 proteins enriched and 14 proteins attenuated in the anterior suture samples compared with adjacent nonsuture regions. In posterior sections, there were 56 proteins enriched and 60 proteins less abundant in the suture region compared with adjacent nonsuture region. A list of enriched and attenuated proteins in suture regions identified by LC-MS/MS can be found in the Supplementary Table S2.

Hierarchical clustering was performed for statistically significantly changed proteins between regions (proteins are listed in Supplementary Table S2). The results can be visualized in the heatmap figures (Figs. 6A, 6B) showing well-segregated dendrograms between the suture and nonsuture regions. The differentially expressed proteins clearly distinguish two distinct, spatially adjacent regions. GO enrichment analysis of differentially represented proteins against the background of all quantified proteins were performed (Figs. 6A, 6B). The GO terms "cell–cell adhesion" and "adherens junction" were highly represented among the proteins enriched in both anterior and posterior suture regions. Proteins contributing to the enrichment of adherens junctions include CDH2, ARVCF, catenin α2 (CTNNA2), catenin β1 (CTNNB1), integrin subunit beta 1 (ITGB1), neuronal cell adhesion molecule, flotillin 2 (FLOT2), and CD46. Other enriched GO terms in suture regions include regulation to response to stimulus, recycling endosome, and cell–matrix adhesion in the anterior and regulation of cell migration, cell morphogenesis, signal transducer activity, cell–substrate adhesion, and catenin complex in the posterior. No statistically significant enriched GO terms were identified from the proteins that were attenuated in the anterior suture region, but glycolysis was attenuated in the posterior suture represented by reduced levels of glucose catabolism enzymes (GPI, ALDOA, ALDOC, GAPDH, PGAM1, PGK1, TPI1, and ENO1), indicating decreased catabolic activity close to the fiber cell tips.

Immunofluorescence

In contrast with our IMS and LC-MS/MS results, decreased cadherin signals at lens sutures was previously reported based on decreased immunolabelling of cadherin.[2] Immunofluorescence was also performed in this study to confirm our IMS and LC-MS/MS data. The results from CDH2 immunolabeling can be found in Figures 7A and 7B, showing increased CDH2 immunolabeling at suture branches. Immunofluorescence was also conducted on fresh frozen sections (Figs. 7C, 7D) and increased CDH2 signal at the sutures is apparent. Therefore, our results from immunofluorescence of CDH2 are consistent with IMS and LC-MS/MS analysis. The distribution of connexin 50 surrounding the sutures was also studied by immunoflu-

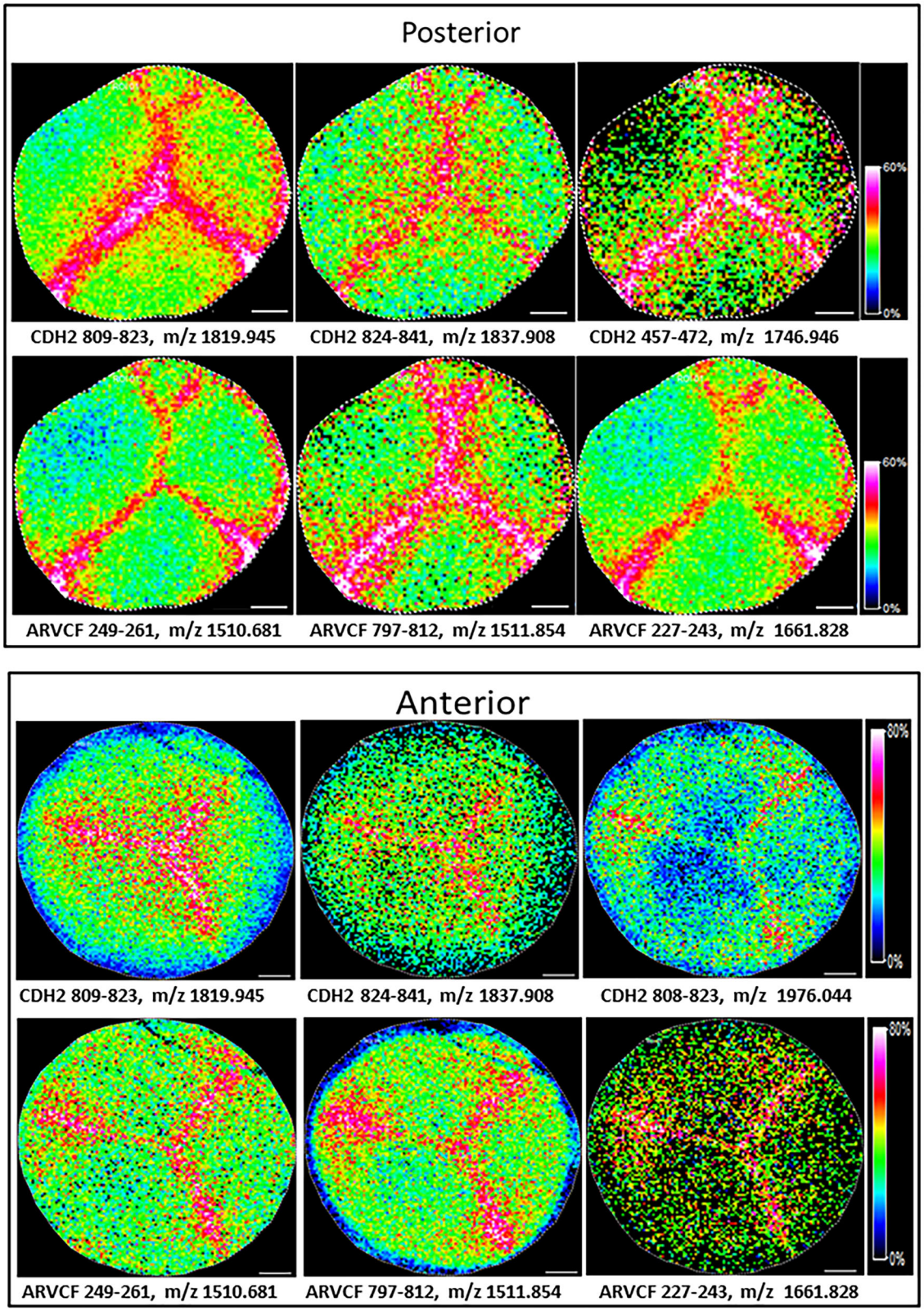

Figure 2. MALDI images of CDH2 and ARVCF peptides. Images of three unique peptides from CDH2 and ARVCF normalized by root-mean-square (RMS). Increased abundance of CDH2 and ARVCF at the sutures was detected. Scale bar, 1 mm

orescence to understand the discrepancy of our IMS data and LC-MS/MS quantification. The immunofluorescence results shown in Figure 8 confirmed decreased connexin 50 immunolabeling at the suture branches in both anterior and posterior sections. The sections were also co-stained with wheat germ agglutinin to show the presence of the cell

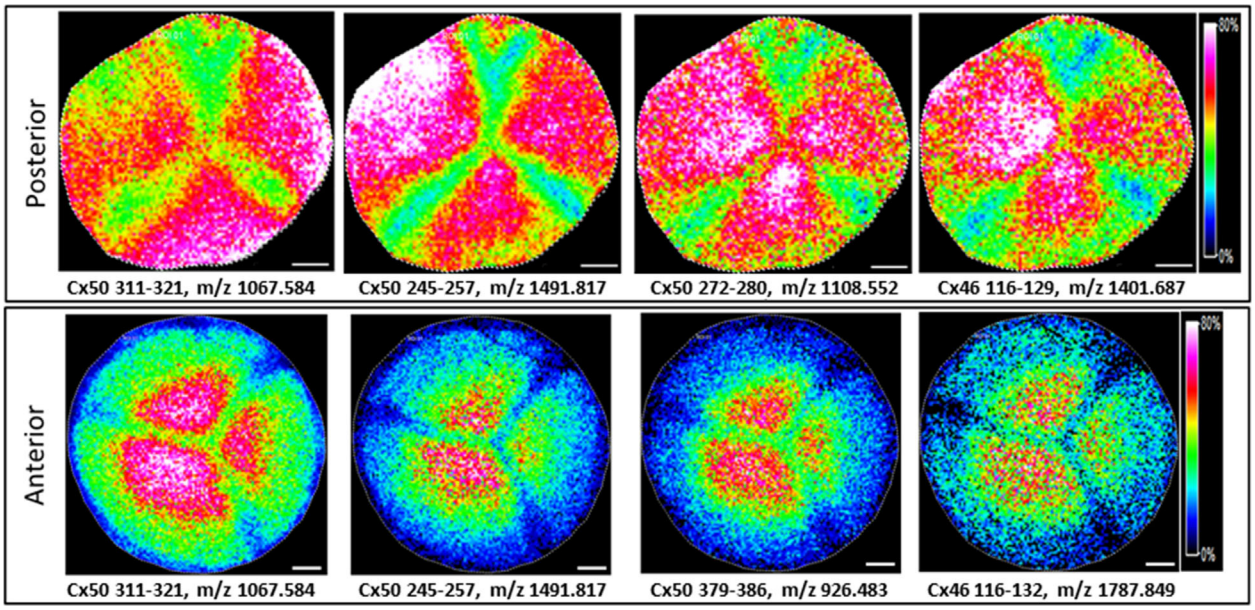

Figure 3. MALDI images of connexin 50 (Cx50) and connexin 46 (Cx46) peptides. Images of connexin 50 and connexin 46 peptides normalized by root-mean-square (RMS). Signals from both connexin 50 and connexin 46 decreased in the suture regions. Scale bar, 1 mm.

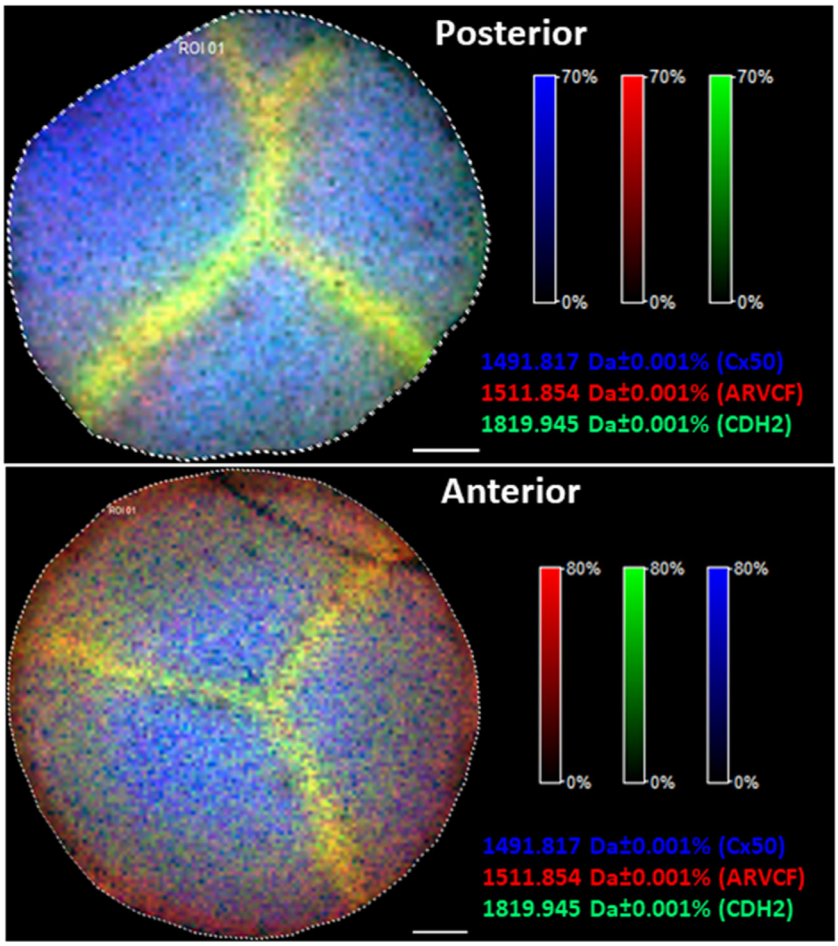

Figure 4. Overlay of connexin 50 (Cx50), cadherin (CDH2), and ARVCF signals. Overlay of MALDI images show inversely correlated expression of adherens junction proteins (N-cadherin [*green*] and ARVCF [*r*ed]) and complementary expression of gap junction protein connexin 50 [*blue*]). Scale bar, 1 mm.

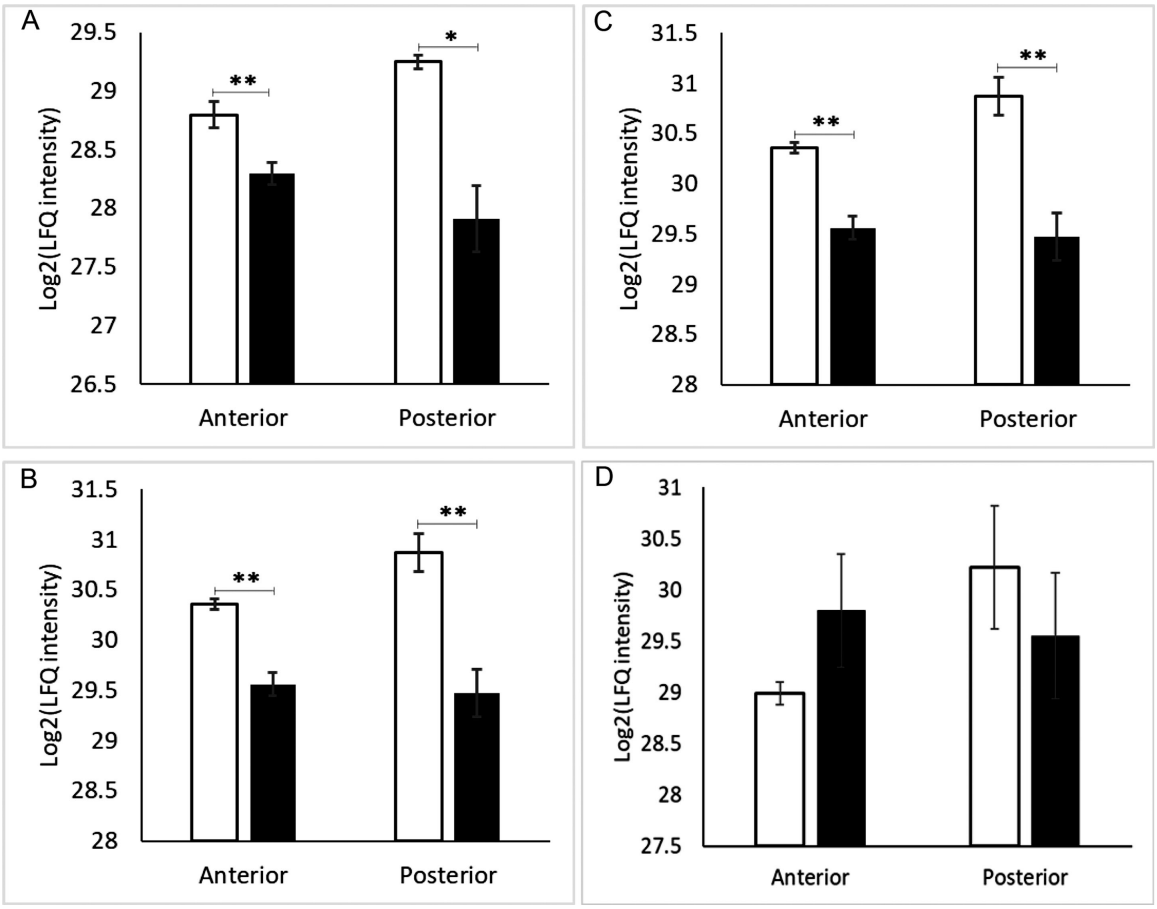

Figure 5. LFQ intensity of CDH2, ARVCF, Cx50, and Cx46 in the suture and suture adjacent regions. LFQ intensities of CDH2, ARVCF, Cx50, and Cx46 were Log2 transformed, and Student t-tests were performed. The abundance of ARVCF (**A**) and CDH2 (**B**) increases in the suture regions (*white bars*) compared with adjacent regions (*black bars*) in both anterior and posterior regions of the lens. The abundance of Cx50 (**C**) decreased in the suture regions (*white bars*) compared with adjacent regions (*black bars*) in the anterior of the lens. The same trend was also detected for Cx46, but the difference did not reach statistical significance. Both Cx50 (**C**) and Cx46 (**D**) in posterior region did not significantly change between the two LCM captured regions. $^{*}P < 0.05$, $^{**}P < 0.005$.

membrane at the suture branches. The strong wheat germ agglutinin signal at the suture branches confirmed the dark regions in Cx50 immunolabeling were not due to tissue damage. The immunofluorescence analysis showed the regions with attenuated connexin 50 signals have a width of approximately 120 to 150 µm in the anterior region and 50 to 60 µm in the posterior region. In addition, stronger connexin 50 labeling was detected immediately adjacent to the suture compared with more distant nonsuture regions. This result suggests that LCM captured suture samples from the posterior sections contained the suture region and a region that contains highly abundant connexins and explains the discrepancy between our IMS data and LC-MS/MS data. Co-labeling of CDH2 and Cx50 was also conducted (Supplementary Fig. S5), revealing a more pronounced CDH2 signal in the suture regions compared with nonsuture regions. In nonsuture regions, Cx50 signal exhibited a uniform distribution, whereas in the suture regions, only a sparse Cx50 signal was detectable.

Discussion

Lens fiber cells are organized in a highly ordered manner and the precise packing of fiber cells relies on extensive intercellular adhesion complexes.[36,37] Cell–cell adhesions not only stabilize this ordered structure to maintain lens transparency, but also play important roles for holding cells together during accommodation.[37] Suture organization was found to be particularly related to accommodative ability of the lens.[4,38] Importantly, previous work has not identified cell junction complexes at sutures.[26] Al-Ghoul et al.[26] reported the presence of a terminal web on either side of sutures that stabilizes fiber ends both within and between growth shells; however, they found decreased cadherin signal at sutures.[2] Transmission electron microscopy also showed relatively loose cell attachment at sutures.[38] Therefore, Lu et al.[2] predicted that sutures may simply be composed of structural interdigitations, because adhesion molecules were not detected. In contrast with the report from Lu et al., results from the current study support the enrichment of major adherens junction proteins such as CDH2, ARVCF, CTNNA2, and CTNNB1 at lens suture branches, suggesting the presence of adherens junction at sutures. Adherens junctions are believed to be involved in stabilizing the structural integrity of lens cells during accommodation and in preserving a specific lens shape.[39] It is not surprising, therefore, to find that fiber cells also use adherens junctions to maintain lens structural integrity in

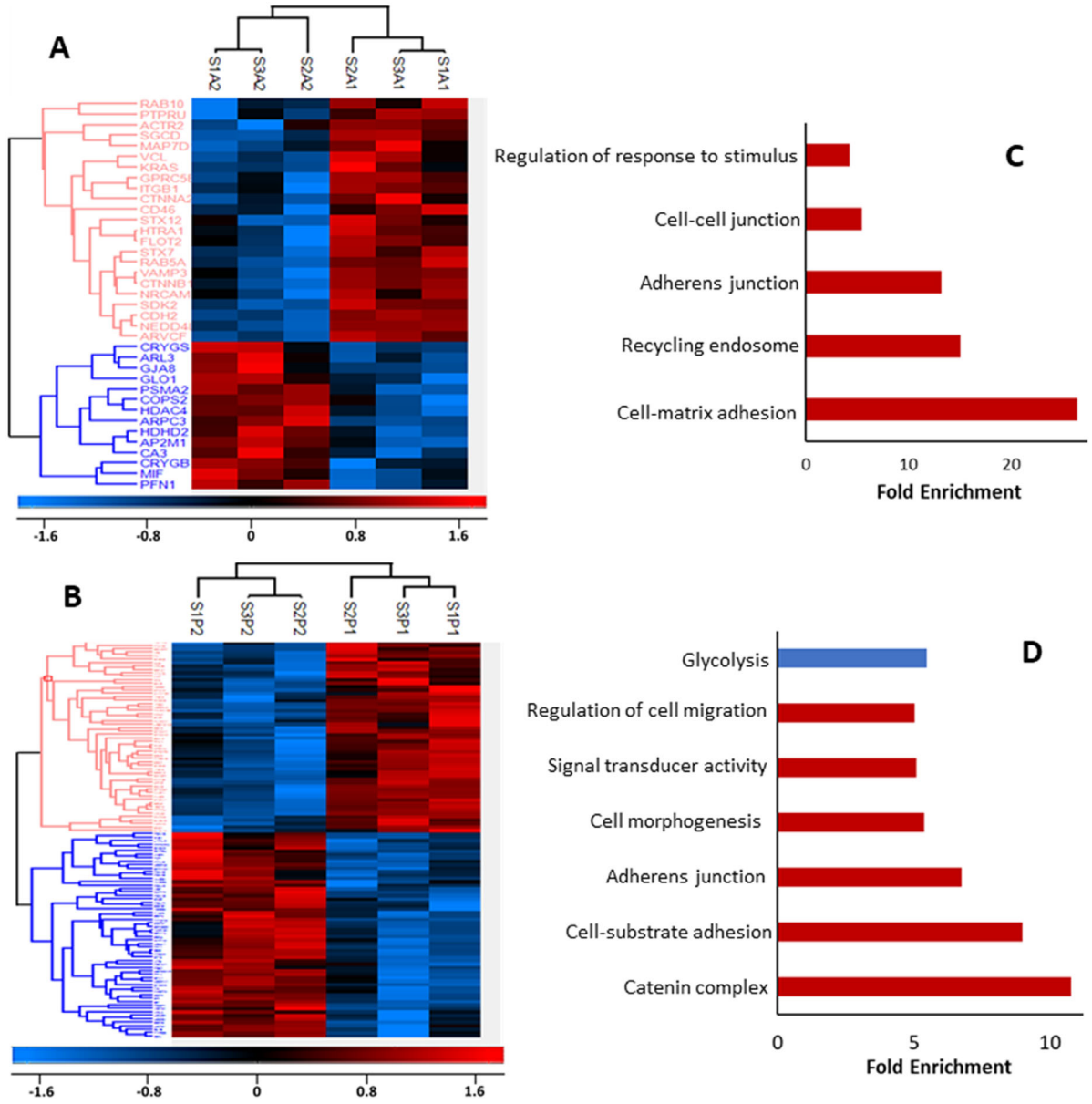

Figure 6. Heatmap and hierarchical clustering and GO terms enrichment analysis. Hierarchical clustering for statistically significant changed proteins ($P < 0.05$) between suture and suture adjacent regions. S1A1, S2A1, and S3A1 and S1P1, S2P1, and S3P1 are three biological replicates for suture regions and S1A2, S2A2, S3A2 and S1P2, S2P2, S3P2 are three biological replicates for suture adjacent regions. Hierarchical clustering defined two clusters of proteins for each comparison (**A**, anterior; **B**, posterior). Note that all proteins shown in **A** and **B** are listed in Supplementary Table S2. Enriched GO terms in each of these clusters are shown on the *right* (**C**, **D**). *Blue* and *red bars* represent GO terms that are decreased or increased in suture region, respectively.

suture region. Lu et al. also reported decreased β1 integrin signal at the suture branches in rat[2]; however, our LCM data showed β1 integrin expression was also increased at sutures. Strong β1 integrin signal at sutures was also reported previously.[40] Previously, the cadherin distribution along the anterior–posterior fiber length was reported as differing between species,[2] and it is not known if a species difference could also contribute the different cadherin and β1 integrin distributions at suture branches reported by Lu et al. and in the current study.

Cadherins are transmembrane proteins that mediate calcium-dependent intercellular adhesion in epithelial and endothelial cells.[41] Both E-cadherin and N-cadherin are expressed in undifferentiated lens epithelial cells during lens development[42]; however, E-cadherin expression is abrogated during fiber cell differentiation.[43] Fully differentiated fiber cells rely on N-cadherin junctions to organize fiber cell lateral interfaces[43]; however, lateral contacts between fiber cells are not disrupted in lens-specific N-cadherin conditional knockout mouse.[43] These results suggest that forming adherens junction along the lateral interfaces may not be the major role of N-cadherin in lens. Logan et al.[43] have reported that N-cadherin junctions were enriched specifically in the apical regions of newly differentiating secondary fiber cells and were required for the migration of the apical tips of newly differentiating fiber cells along the epithelial cell–fiber

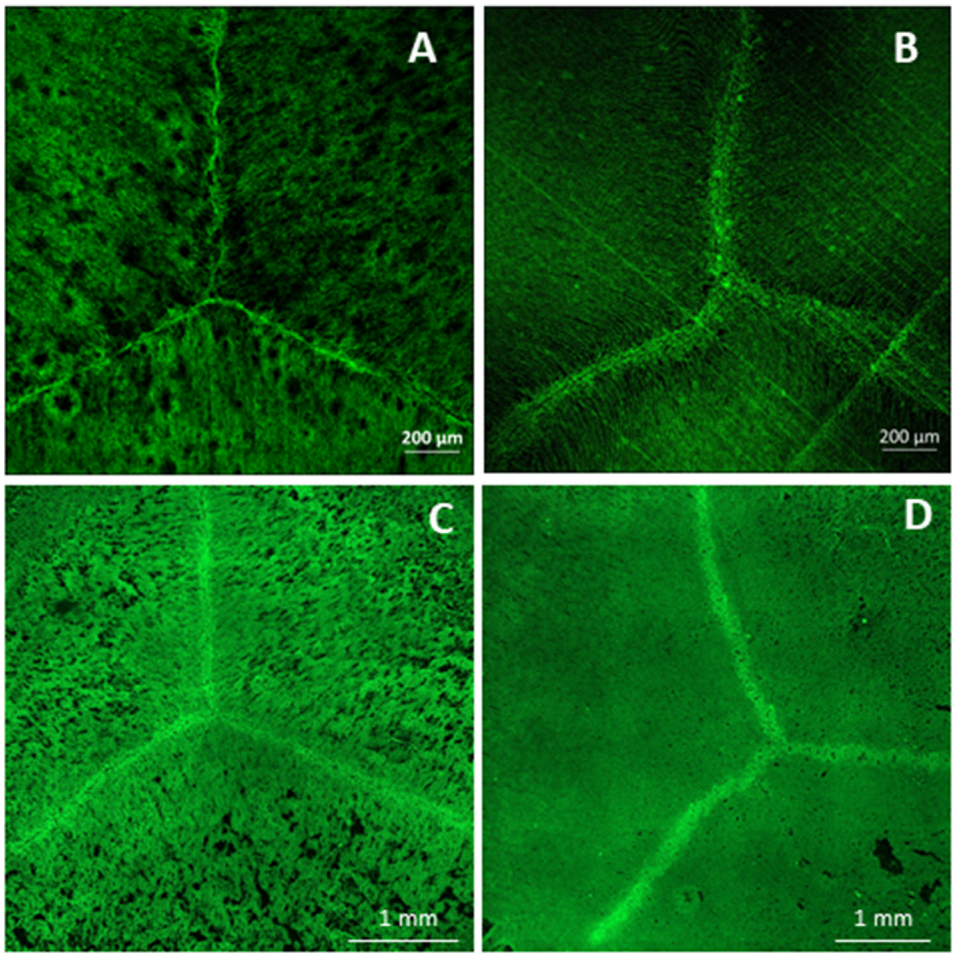

Figure 7. Immunofluorescence of CDH2. Sections were obtained from either anterior (**A**, **C**) or posterior regions (**B**, **D**) in fixed bovine lenses (**A**, **B**) or fresh frozen bovine lenses (**C**, **D**). The sections were immunolabeled with anti- CDH2 antibodies. Images were obtained using either a Zeiss LSM 880 confocal laser scanning microscope (**A**, **B**) or a Zeiss Axioscan.Z1 (**C**, **D**). The results showed increased CDH2 signal at suture branches. (**A**, **B**) Scale bars, 200 µm. (**C**, **D**) Scale bars, 1 mm.

cell interface. Our results indicate that N-cadherin was also enriched in the mature fiber cell tips.

In addition to N-cadherin, ARVCF, a member of the catenin family, was also enriched in the fiber cell tips. ARVCF is strongly expressed in lens fiber cells, and it is highly phosphorylated.[44,45] Recently, ARVCF was reported to be essential for maintaining lens transparency and ARVCF-deficient mouse lenses developed age-related cortical cataracts.[46] In addition, opacities along the suture line and altered mechanical properties in ARVCF-deficient mice were also reported.[46] ARVCF belongs to the cadherin–catenin complex, and it binds to the juxtamembrane domain of cadherins and may modulate cadherin-mediated cell–cell junctions.[47] Therefore, it is not surprising to detect the same distribution of cadherin and ARVCF. Enriched major adherens junction protein cadherin and ARVCF, along with many other proteins that belong to adherens junctions, strongly supports the presence of adherens junctions at sutures.

Gap junctions are mostly distributed near the equatorial region, which is thought to effectively facilitate the outward flow of current toward the equatorial surface as a component of the lens microcirculation system.[48,49] It has been proposed that gap junctions are not responsible for connecting fiber cells across lens sutures[2]; however, detailed characterization of gap junctions in suture regions has not been reported. In this study, IMS data showed decreased gap junction protein connexin 50 and connexin 46 in the suture regions. Immunofluorescence results also confirmed reduced connexin 50 signals at lens sutures. These results confirmed the previous report of lack of gap junctions across sutures.[2]

Lens sutures play an important role in the lens microcirculation model for transporting nutrients extracellularly to the center of the lens.[50,51] Other than forming gap junctions with narrow intercellular gaps, adherens junctions at lens sutures may better facilitate extracellular transport. Adherens junctions undergo assembly or disassembly, which can be regulated by external or internal forces, cell signal transduction, and facilitated by the interaction with the cytoskeleton.[52,53] For example, phosphorylation acts as a switch for the majority of adherens junction proteins by regulating protein–protein interactions.[52] Our LCM-LC-MS/MS data showed receptor-type tyrosine-protein phosphatase U, a protein regulating phosphorylation of CTNNB1, was found to be enriched in the suture region. In addition, adherens junctions can change their mechanical strength, signaling potentials, and junctional intercellular distance by changing cadherin/catenin complex distribution and internal

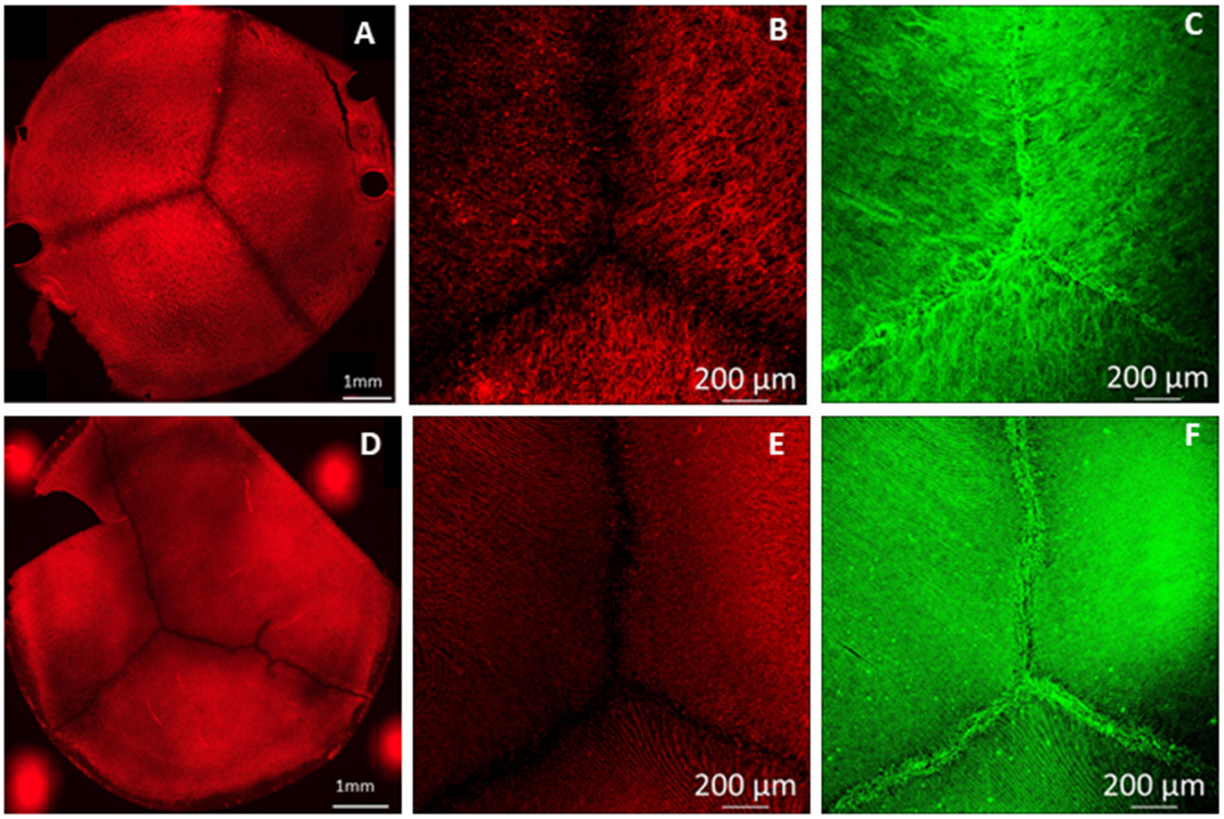

Figure 8. Immunofluorescence of connexin 50. Sections were obtained from either anterior (**A**, **B**, **C**, 400–600 µm from the epithelial cell–fiber cell interface [EFI]) or posterior regions (**D**, **E**, **F**, 400–600 µm from CFI) in fixed bovine lenses. The sections were immunolabeled with anti-connexin 50 antibodies (**A**, **B**, **D**, **E**) and wheat germ agglutinin (**C**, **F**). Both low-magnification images (**A**, **D**) and high-magnification images (**B**, **E**) show decreased connexin 50 immunolabeling at suture branches. Wheat germ agglutinin labeling (**C**, **F**) shows the presence of cell membrane in the suture region.

organization.[53] Therefore, with highly, dynamically regulated junctions, lens sutures could fulfill the functions required for both accommodation and extracellular nutrition transport.

In addition to verifying IMS results, LC-MS/MS analysis detected many interesting proteins that were enriched in the fiber tips. EPHA2 was found to be significantly enriched in the fiber tips in the posterior sections. EPHA2 has recently been reported to be needed for normal patterning of fiber cell tips and the formation of a well-aligned Y-suture.[54] Nance-Horan syndrome protein, a protein that is associated with severe bilateral cataracts,[55] was also found increased in the posterior sutures. The protein RAC1 that was reported to link to defects in suture formation[56] was also found enriched in posterior suture. Another two interesting proteins enriched in sutures are sidekick cell adhesion molecule 1 (SDK1) and 2 (SDK2). SDKs were initially identified as genes required for pattern formation in the *Drosophila* eye.[57] Later, as synaptic adhesion molecules, SDKs were found to mediate laminar targeting of specific neurons in the retina.[58] The lamina specificity was achieved through mutually exclusive expression of SDK1 and SDK2 and homophilic adhesion mediated by SDKs.[58] Considering the important function of SDKs in directing proper neuronal targeting mediated by homophilic adhesion, they may also play important roles in guiding precise end to end arrangement of lens fiber cells. Because both SDK1 and SDK2 are detected in the sutures, it is expected there will be at least two different recognitions when the fiber cells abut and overlap. Studying SDK spatial distribution in fiber cells tips will provide valuable information toward understanding the suture formation. Based on the results from LC-MS/MS analyses, further studies to search proteins and posttranslational modifications that could regulate cell–cell adhesion and extracellular transport at sutures are underway.

Acknowledgments

Support by National Institutes of Health by grants R01 EY013462 and P30 EY008126. Support from the Proteomics and Tissue Imaging Core Facilities of the Vanderbilt University Mass Spectrometry Research Center is also acknowledged.

Disclosure: **Z. Wang**, None; **R.B. Gletten**, None; **K.L. Schey**, None

References

1. Wride MA. Cellular and molecular features of lens differentiation: a review of recent advances. *Differentiation*. 1996;61:77–93.
2. Lu JY, Mohammed TA, Donohue ST, Al Ghoul KJ. Distribution of basal membrane complex components in elongating lens fibers. *Mol Vis*. 2008;14:1187–1203.
3. Kuszak JR. The development of lens sutures, *Prog Retinal Eye Res*. 1995;14:567–591.

4. Kuszak JR, Zoltoski RK, Tiedemann CE. Development of lens sutures. *Int J Dev Biol*. 2004;48:889–902.
5. Kuszak JR, Peterson KL, Herbert KL, Sivak JG. The interrelationship of lens anatomy and optical quality. II. Primate lenses. *Expl Eye Res*. 1994;59:521–536.
6. Bassnett S, Winzenburger PA. Morphometric analysis of fibre cell growth in the developing chicken lens, *Exp Eye Res*. 2003;76:291–302.
7. Kuszak JR, Sivak JG, Weerheim JA. Lens optical quality is a direct function of lens sutural architecture. *Invest Ophthalmol Vis Sci*. 1991;32:2119–2129.
8. Taylor VL, al-Ghoul KJ, Lane CW, Davis VA, Kuszak JR, Costello MJ. Morphology of the normal human lens. *Invest Ophthalmol Vis Sci*. 1996;37:1396–1410.
9. Wenke JL, McDonald WH, Schey KL. Spatially directed proteomics of the human lens outer cortex reveals an intermediate filament switch associated with the remodeling zone. *Invest Ophthalmol Vis Sci*. 2016;57:4108–4114.
10. Wang Z, Cantrell LS, Schey KL. Spatially resolved proteomic analysis of the lens extracellular diffusion barrier, *Invest Ophthalmol Vis Sci*. 2021;62:25.
11. Gangalum RK, Kim D, Kashyap RK, et al. Spatial analysis of single fiber cells of the developing ocular lens reveals regulated heterogeneity of gene expression. *iScience*. 2018;10:66–79.
12. Stella DR, Floyd KA, Grey AC, Renfrow MB, Schey KL, Barnes S. Tissue localization and solubilities of αA-crystallin and its numerous C-terminal truncation products in pre- and post-cataractous ICR/f rat lenses. *Invest Ophthalmol Vis Sci*. 2010;51:5153–5161.
13. Grey AC, Schey KL. Age-related changes in the spatial distribution of human lens α-crystallin products by MALDI imaging mass spectrometry. *Invest Ophthalmol Vis Sci*. 2009;50:4319–4329.
14. Grey AC, Schey KL. Distribution of bovine and rabbit lens α-crystallin products by MALDI imaging mass spectrometry. *Mol Vis*. 2008;14:171–179.
15. Garland DL, Duglas-Tabor Y, Jimenez-Asensio J, Datiles MB, Magno B. The nucleus of the human lens: demonstration of a highly characteristic protein pattern by two-dimensional electrophoresis and introduction of a new method of lens dissection. *Exp Eye Res*. 1996;62:285–291.
16. Asomugha CO, Gupta R, Srivastava OP. Identification of crystallin modifications in the human lens cortex and nucleus using laser capture microdissection and CyDye labeling, *Mol Vis*. 2010;16:476–94.
17. Wenke JL, Rose KL, Spraggins JM, Schey KL. MALDI imaging mass spectrometry spatially maps age-related deamidation and truncation of human lens aquaporin-0. *Invest Ophthalmol Vis Sci*. 2015;56:7398–7405.
18. Gutierrez DB, Garland DL, Schwacke JH, Hachey DL, Schey KL. Spatial distributions of phosphorylated membrane proteins aquaporin 0 and MP20 across young and aged human lenses. *Exp Eye Res*. 2016;149:59–65.
19. Wang Z, Schey KL. Quantification of thioether-linked glutathione modifications in human lens proteins. *Exp Eye Res*. 2018;175:83–89.
20. Colvis C, Garland D. Posttranslational modification of human alphaA-crystallin: correlation with electrophoretic migration. *Arch Biochem Biophys*. 2002;397:319–323.
21. Vaghefi E, Pontre BP, Jacobs MD, Donaldson PJ. Visualizing ocular lens fluid dynamics using MRI: manipulation of steady state water content and water fluxes. *Am J Physiol Regul Integr Comp Physiol*. 2011;301:R335–R342.
22. Vaghefi E, Walker K, Pontre BP, Jacobs MD, Donaldson PJ. Magnetic resonance and confocal imaging of solute penetration into the lens reveals a zone of restricted extracellular space diffusion. *Am J Physiol Regul Integr Comp Physiol*. 2012;302:R1250–R1259.
23. Zampighi GA, Eskandari S, Kreman M. Epithelial organization of the mammalian lens. *Exp Eye Res*. 2000;71:415–435.
24. Al-Ghoul KJ, Kirk T, Kuszak AJ, Zoltoski RK, Shiels A, Kuszak JR. Lens structure in MIP-deficient mice. *Anat Rec A Discov Mol Cell Evol Biol*. 2003;273:714–730.
25. Fan J, Lerner J, Wyatt MK, et al. The klotho-related protein KLPH (lctl) has preferred expression in lens and is essential for expression of clic5 and normal lens suture formation. *Exp Eye Res*. 2018;169:111–121.
26. Al-Ghoul KJ, Lindquist TP, Kirk SS, Donohue ST. A novel terminal web-like structure in cortical lens fibers: architecture and functional assessment, *Anat Rec (Hoboken)*. 2010;293:1805–1815.
27. Caprioli RM, Farmer TB, Gile J. Molecular imaging of biological samples: localization of peptides and proteins using MALDI-TOF MS. *Anal Chem*. 1997;69:4751–4760.
28. Franck J, Longuespée R, Wisztorski M, et al. MALDI mass spectrometry imaging of proteins exceeding 30,000 daltons. *Med Sci Monit*. 2010;16:BR293–BR299.
29. Judd AM, Gutierrez DB, Moore JL, et al. A recommended and verified procedure for in situ tryptic digestion of formalin-fixed paraffin-embedded tissues for analysis by matrix-assisted laser desorption/ionization imaging mass spectrometry. *J Mass Spectrom*. 2019;54:716–727.
30. Wang Z, Ryan DJ, Schey KL. Localization of the lens intermediate filament switch by imaging mass spectrometry *Exp Eye Res*. 2020;198:108134.
31. Gletten RB, Cantrell LS, Bhattacharya S, Schey KL. Lens aquaporin-5 inserts into bovine fiber cell plasma membranes via unconventional protein secretion. *Invest Ophthalmol Vis Sci*. 2022;63:5.
32. Cox J, Hein MY, Luber CA, Paron I, Nagaraj N, Mann M. Accurate proteome-wide label-free quantification by delayed normalization and maximal peptide ratio extraction, termed MaxLFQ. *Mol Cell Proteomics*. 2014;13:2513–2526.
33. Cox J, Neuhauser N, Michalski A, Scheltema RA, Olsen JV, Mann M. Andromeda: a peptide search engine integrated into the MaxQuant environment. *J Proteome Res*. 2011;10:1794–1805.
34. Guo G, Papanicolaou M, Demarais NJ, et al. Automated annotation and visualisation of high-resolution spatial proteomic mass spectrometry imaging data using HIT-MAP. *Nat Commun*. 2021;12:3241.
35. Grey AC, Chaurand P, Caprioli RM, Schey KL. MALDI imaging mass spectrometry of integral membrane proteins from ocular lens and retinal tissue. *J Proteome Res*. 2009;8:3278–3283
36. Cooper MA, Son AI, Komlos D, Sun Y, Kleiman NJ, Zhou R. Loss of ephrin-A5 function disrupts lens fiber cell packing and leads to cataract. *Proc Natl Acad Sci USA*. 2008;105:16620–16625.
37. Beebe DC, Vasiliev O, Guo J, Shui Y, Bassnett S. Changes in adhesion complexes define stages in the differentiation of lens fiber cells. *Invest Ophthalmol Vis Sci*. 2001;42:727–734.
38. Kuszak JR, Mazurkiewicz M, Jison L, Madurski A, Ngando A, Zoltoski RK. Quantitative analysis of animal model lens anatomy: accommodative range is related to fiber structure and organization. *Vet Ophthalmol*. 2006;9:266–280.
39. Lo W-K. Adherens junctions between cortical fiber cells of the ocular lens. *Invest Ophthamol Vis Sci*. 1987;28:83.
40. Wederell ED, Brown H, O'Connor M, Chamberlain CG, McAvoy JW, de Iongh RU. Laminin-binding integrins in rat lens morphogenesis and their regulation during fibre differentiation. *Exp Eye Res*. 2005;81:326–339.
41. Nawijn MC. E-cadherin: gatekeeper of airway mucosa and allergic sensitization. *Trends Immunol*. 2011;32:248–255.

Investigative Ophthalmology & Visual Science

42. Leonard M, Zhang L, Zhai N, et al. Modulation of N-cadherin junctions and their role as epicenters of differentiation-specific actin regulation in the developing lens. *Dev Biol*. 2011;349:363–377.
43. Logan CM, Rajakaruna S, Bowen C, Radice GL, Robinson ML, Menko AS. N-cadherin regulates signaling mechanisms required for lens fiber cell elongation and lens morphogenesis. *Dev Biol*. 2017;428:118–134.
44. Wang Z, Han J, David LL, Schey KL. Proteomics and phosphoproteomics analysis of human lens fiber cell membranes. *Invest Ophthalmol Vis Sci*. 2013;54:1135–1143.
45. Zhao Y, Wilmarth PA, Cheng C, et al. Proteome-transcriptome analysis and proteome remodeling in mouse lens epithelium and fibers. *Exp Eye Res*. 2019;179:32–46.
46. Martin JB, Herman K, Houssin NS, Rich W, Reilly MA, Plageman TF, Jr. ARVCF dependent adherens junction stability is required to prevent age-related cortical cataracts. *Front Cell Dev Biol*. 2022;10:840129.
47. Kaufmann U, Zuppinger C, Waibler Z, et al. The armadillo repeat region targets ARVCF to cadherin-based cellular junctions. *J Cell Sci*. 2000;113:4121–4135.
48. Biswas SK, Lee JE, Brako L, Jiang JX, Lo WK. Gap junctions are selectively associated with interlocking ball-and-sockets but not protrusions in the lens. *Mol Vis*. 2010;6:2328–2341.
49. Baldo GJ, Mathias RT. Spatial variations in membrane properties in the intact rat lens. *Biophys J*. 1992;63:518–529.
50. Vaghefi E, Donaldson PJ. The lens internal microcirculation system delivers solutes to the lens core faster than would be predicted by passive diffusion. *Am J Physiol Regul Integr Comp Physiol*. 2018;315:R994–R1002.
51. Mathias RT, Rae JL, Baldo GJ. Physiological properties of the normal lens. *Physiol Rev*. 1997;77:21–50.
52. Bertocchi C, Rao MV, Zaidel-Bar R. Regulation of adherens junction dynamics by phosphorylation switches. *J Signal Transduct*. 2012;2012:125295.
53. Troyanovsky S. Adherens junction assembly. *Subcell Biochem*. 2012;60:89–108.
54. Cheng C. EphA2 and ephrin-A5 guide eye lens suture alignment and influence whole lens resilience. *Invest Ophthalmol Vis Sci*. 2021;62:3.
55. Horan MB, Billson FA. X-linked cataract and hutchinsonian teeth. *J Paediatr Child Health*. 1974;10:98–102.
56. Maddala R, Chauhan BK, Walker C, et al. Rac1 GTPase-deficient mouse lens exhibits defects in shape, suture formation, fiber cell migration and survival. *Dev Biol*. 2011;360:30–43.
57. Nguyen DN, Liu Y, Litsky ML, Reinke R. The sidekick gene, a member of the immunoglobulin superfamily, is required for pattern formation in the Drosophila eye. *Development*. 1997;124:3303–3312.
58. Yamagata M, Weiner JA, Sanes JR. Sidekicks: synaptic adhesion molecules that promote lamina-specific connectivity in the retina. *Cell*. 2002;110:649–660.

Investigative Ophthalmology & Visual Science